

# Near Vertical Incidence Skywave Propagation: Elevation Angles and Optimum Antenna Height for Horizontal Dipole Antennas

**Ben A. Witvliet<sup>1,2</sup>, Erik van Maanen<sup>2</sup>, George J. Petersen<sup>2</sup>, Albert J. Westenberg<sup>2</sup>, Mark J. Bentum<sup>1</sup>, Cornelis H. Slump<sup>1</sup>, and Roel Schiphorst<sup>1</sup>**

<sup>1</sup>Center for Telecommunications and Information Technology, University of Twente,  
7500 AE Enschede, The Netherlands  
E-mail: b.a.witvliet@utwente.nl

<sup>2</sup>Radiocommunications Agency Netherlands,  
9700 AL Groningen, The Netherlands  
E-mail: ben.witvliet@agentschaptelecom.nl

---

## Abstract

Near Vertical Incidence Skywave (NVIS) communication uses the ionosphere as a reflector to cover a continuous area with a radius of at least 150 km around the transmitter, on frequencies typically between 3 and 10 MHz. In developing countries, in areas lacking any other telecommunication infrastructure, it is used on a daily basis for voice and data communication. It may also be used in ad-hoc emergency (disaster) communication in other regions. This paper proposes optimum heights above ground for horizontal dipole antennas for NVIS, based on simulations and empirical data. First, the relationship between elevation angle and skip distance is obtained using ionospheric ray tracing. The high elevation angles found by simulation are confirmed by elevation angle measurements using a professional radio direction finder. The measurements also show the dominance of NVIS over ground wave propagation starting at a short distance. For these elevation angles, the optimum receive and transmit antenna heights above ground are derived using antenna simulations. A distinction is made between optimum transmit signal strength and optimum received signal-to-noise ratio (SNR). These optima are verified experimentally, demonstrating a novel evaluation method that can be used in the presence of the fading typical for ionospheric propagation. For farmland soil ( $\sigma \approx 20$  mS/m,  $\epsilon_r \approx 17$ ) the optimum height above ground for the transmit antenna is  $0.18\text{--}0.22\lambda$ . If the antenna is lowered to  $0.02\lambda$  a transmit signal loss of 12 dB occurs. This corresponds with the theory. The receive antenna height, however, while appearing uncritical in the simulations, showed a clear optimum at  $0.16\lambda$  and a 2–7 dB SNR deterioration when lowered to  $0.02\lambda$ .

Keywords: Antenna height; antenna radiation patterns; dipole antennas; elevation angle; ionosphere; Near Vertical Incident Skywave (NVIS); radio wave propagation; receiving antennas; signal-to-noise ratio (SNR); transmitting antennas

## 1. Introduction

Near Vertical Incident Skywave (NVIS) radio wave propagation uses the ionosphere as a reflector, on frequencies ranging from approximately 3 to 10 MHz. While high-frequency (HF: 3–30 MHz) radio communication has ceded its role in

daily European and North American life to satellite communication and cellular networks, it still thrives in more challenging ad-hoc situations, such as disaster relief and military operations [1]. NVIS propagation is also used on a daily basis in developing countries, in areas where telecommunication networks are unreliable or nonexistent, providing essential telecommunication, such as voice and data communication between small business offices, healthcare facilities, and even banking facilities. It may also be used on an ad-hoc basis in disaster relief communications,

---

Digital Object Identifier 10.1109/MAP.2015.2397071  
Date of publication: 24 February 2015

providing a quickly deployable alternative to destroyed telecommunication infrastructure in natural catastrophes such as the 1953 “Big Flood” in The Netherlands [2, 3], the 2005 flooding of New Orleans, and the 2011 tsunami in Japan. To cover an area around and directly adjacent to the transmitter, electromagnetic waves must be launched at steep angles, entering the ionosphere nearly perpendicularly, hence the prefix “Near Vertical Incidence”. In the ionosphere, the electromagnetic waves are reflected back to earth, after which they land in an umbrellalike fashion in the area around the transmitter, as is illustrated in Figure 1.

If a suitable frequency is selected, a single 100-W NVIS base station can cover an area with a 150-km radius with good signal strength, exceeding  $50 \text{ dB}\mu\text{V}$  on a half-wave dipole antenna. Covering such a large area using ultrahigh frequencies (UHF: 300–3000 MHz) would require a large number of base stations and interlinks. For vital telecommunication in remote areas in developing countries, relatively low cost equipment similar to those marketed for the amateur radio service is used, providing reasonable transmission quality and high receiver sensitivity. The fading, dispersion, and noise typical for ionospheric radio channels add specific requirements to data communication, but advanced modulation techniques and Automatic Repeat Request (ARQ) protocols have been designed for these channels and turn out to be very effective [4].

### 1.1 NVIS Antenna

The NVIS antenna, which is probably the most important element in the radio link, may consist of a simple wire structure and can be cheap and efficient, provided that sufficient knowledge is available to engineer and install these antennas optimally. Optimizing the antenna radiation pattern for NVIS elevation angles promises significant improvement of the radio communication link. This paper provides measurements and simulations on NVIS elevation angles and optimum antenna height. The focus will be on horizontal half-wave dipole antennas, with a differentiation between optimization for transmission and reception, each having different requirements.

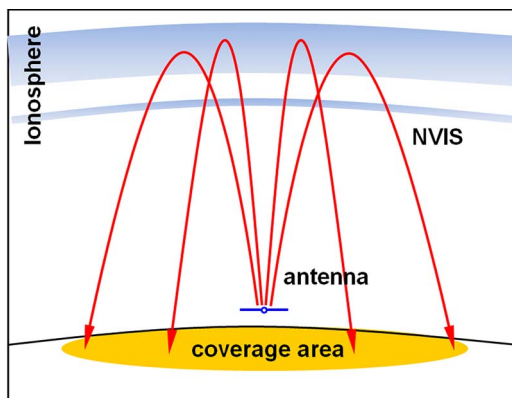


**Figure 1. NVIS: Electromagnetic waves launched nearly vertically are reflected back to earth, after which they land in an umbrellalike fashion in the area around the transmitter.**

An excellent introduction to NVIS radio communication can be found in [5], and the importance of NVIS during field operations is underlined in [1]. The book of Fiedler and Farmer [6], which is often cited in NVIS presentations, emphasizes the necessity to adapt the antenna patterns to the specifics of NVIS propagation and provides practical information on NVIS antennas.

The traditional vertical whip antennas on cars do not perform very well when using NVIS propagation due to the null in their antenna diagram at high elevation angles [7]. Hagn and Van der Laan [8] discuss measurements on whip antennas on military vehicles. For best NVIS performance, they propose tilting the whips in a horizontal or slanted position when stationary. They arrive at effective antenna gain values between  $-17$  and  $-35 \text{ dBi}$  on frequencies from 4 to 8 MHz, which is still quite poor. For mobile NVIS applications, loop antennas are better adapted, although, due to their small size, their instantaneous bandwidth and efficiency are limited at low frequencies. The optimization of the vertical radiation diagram of such antennas remains a challenge, due to the radiation of currents induced in the vehicle body [9]. On large helicopters, these currents may cause unwanted rotor modulation on specific frequencies [10]. On the other hand, these current can be used effectively by creating an NVIS slot antenna in the body of an airplane [11]. A large shipboard loop is described in [12].

When more installation time is available, wire antennas such as dipoles may be used to provide better performance. Research into NVIS field antenna performance has been performed in the 1960s and 1970s by Barker *et al.* [13], in the USA and in the tropical rainforest of Thailand. A RF source towed by an airplane was used to compare the shape of the radiation pattern with simulations [14], and the relative antenna gain at the zenith was compared using an ionospheric sounder [15]. Austin and Murray used a helium-filled balloon (“blimp”) for NVIS antenna measurements [9].

### 1.2 NVIS Reception

NVIS receive antennas must be optimized for best signal-to-noise ratio (SNR) rather than for best antenna gain. Normally, at HF, external noise dominates over receiver noise, defining the reception threshold. Predicted levels for atmospheric, galactic, and man-made noise can be found in [16]. As the levels of man-made noise are highly dependent on electric and electronic equipment quality, equipment density, and geographical distribution, and while these parameters have changed over time, new HF noise measurement campaigns using modern means [17] are desirable. Interesting studies show the nonuniform azimuthal distribution of noise [18, 19], which is important for the understanding of HF receive antenna signal-to-noise performance.

The central topic of this paper is the optimization of transmit and receive antennas for fixed or temporary base stations that use NVIS radio wave propagation. The research concentrates on horizontal half-wave dipole antennas for NVIS coverage of an area with 150-km radius, i.e., the area of a

mid-sized European country or US state. The following contributions are made.

- The relationship between NVIS elevation angle and coverage distance is investigated using ionospheric ray tracing software.
- Elevation angle measurements are performed, involving 85 NVIS stations, proving the dominance of NVIS over ground wave starting at short distances and confirming the high elevation angles involved in NVIS propagation (70°–90°).
- NVIS antenna gain and NVIS directivity are defined, to facilitate NVIS antenna comparison. Optimum antenna heights are proposed for different soil types, based on antenna simulations.
- A novel empirical evaluation method for NVIS antenna performance in the presence of HF fading is introduced and demonstrated. These measurements confirm the optimum transmit antenna heights found by simulation.
- However, the optimum height for the receive antenna (highest SNR) does not conform to the simulated values.

Points for further research are identified.

This paper is structured as follows: Section 2 provides a brief summary on ionospheric radio wave propagation. In Section 3, the relationship between NVIS elevation angle and skip distance is investigated using simulations, which is then verified by experiment. Section 4 discusses the adaptation of NVIS antennas to the properties of NVIS propagation. The research then limits itself to horizontal half-wave dipole antennas above real (lossy) earth and the influence of the antenna suspension height. A differentiation is made between transmit and receive performance. Section 5 introduces a novel empirical method that allows evaluation of NVIS antenna performance *in situ* and using NVIS propagation. Practical implementation of this method is discussed, identifying possible pitfalls and describing practical enhancements that improve accuracy. This method is used to verify the optima that were found by simulation, and the measurement results are discussed in Section 5.3 (for the transmit case) and Section 5.4 (for reception). Section 6 compares the optima found with other research and discusses the applicability of the results to other frequencies, other coverage area size, and other sunspot numbers. The article concludes with a summary of the results and subjects that were identified for further research.

## 2. Ionospheric Radio Wave Propagation

To optimize the NVIS antenna, we have to look into ionospheric radio wave propagation first. An extensive overview on the formation of the ionosphere and the radio wave propagation through it can be found in [20–22]. We will limit ourselves here to a brief summary of the subject, with a focus on the key parameters that are linked to NVIS antenna optimization.

The ionosphere extends from an altitude of approximately 50 km upward to several Earth radii [21]. The ionization is caused by ultraviolet, X-ray, and  $\alpha$  radiation from the sun, balanced by ion depletion due to recombination and diffusion. The resulting vertical ion density profile was first described by Chapman [23]. The lower part of the profile, up to the level of maximum ionization, can be derived in real time from virtual height measurements using an ionosonde [24]. The virtual height of the ionosphere is measured by sending a pulsed radio wave vertically toward the ionosphere and receiving the reflection off the ionosphere. The delay of the signal is used to calculate the virtual height of the ionosphere, which is frequency dependent.

An example ionogram is shown in Figure 2. The ionosphere is birefringent: Appleton and Builder [25] showed by experiment that, under the influence of the earth’s magnetic field, the incoming electromagnetic wave is split into two characteristic waves at the base of the ionosphere. These characteristic waves, namely, the ordinary and extraordinary wave, have circular polarization of opposite sense. They follow a different path through the ionosphere and experience different attenuation and show different behavior [26]. They therefore produce two slightly different traces in the ionogram in Figure 2, which are shown as green and red traces. Multiple reflections between the ionosphere and the ground may cause a secondary set of traces, but the main information is derived from the lower set of traces.

### 2.1 Frequency Dependence of Ionospheric Propagation

Local maxima in the electron density profile at specific heights reflect radio waves, depending on the frequency used.

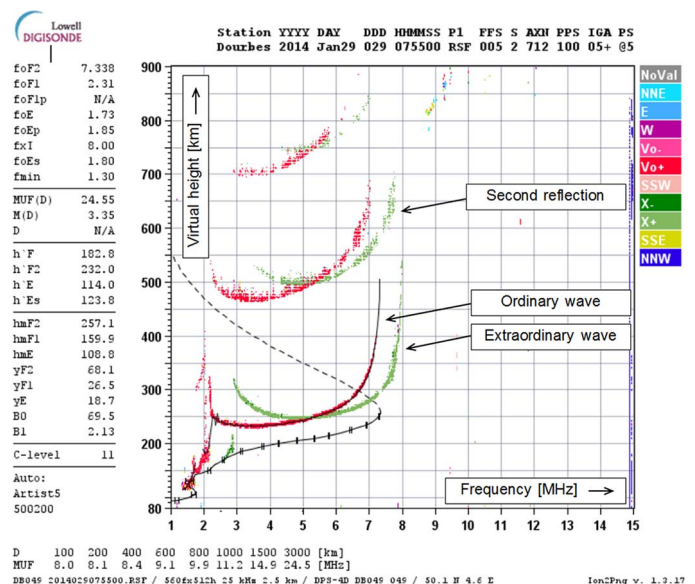


**Figure 2. Ionogram of Dourbes ionosonde (courtesy of Royal Observatory of Belgium) showing the virtual ionospheric height versus frequency on January 29, 2014, 07:55 Coordinated Universal Time (UTC). Red trace represents the ordinary wave; green trace represents the extraordinary wave. Boxed texts are added by the authors.**

These ionospheric regions are referred to as ionospheric “layers”. Each layer has his own characteristics and is indicated with a letter (D, E, and F) starting from the ground upward. The reflection of radio waves against the E and F layers is responsible for most ionospheric radio wave propagation. The D layer is present during daylight hours only and causes attenuation that is inversely proportional to the operating frequency [27]. The E layer may contain local high-density clouds, which are sparse both in occurrence and in localization, indicated as “sporadic E” or “Es”. During daytime, the F layer may split into two regions, namely, a lower and less prominent F1 layer and a higher and denser F2 layer, to merge into one F layer again at night. Diffuse irregularities in the topside ionosphere with high electron density are indicated as “Spread-F” [28].

The highest frequency, at which an electromagnetic wave will be reflected by an ionospheric layer when launched vertically, is called its “plasma frequency” or “critical frequency”. The critical frequency for the ordinary wave is indicated with “fo” followed by the letter representing the layer, e.g., foE, foF1, and foF2. Similarly, the critical frequency of the extraordinary wave is indicated with “fx”, e.g., fxF2. The critical frequency of the extraordinary wave is slightly higher than that of the ordinary wave, the difference being half the electron gyro frequency. The key parameters of the different layers are shown at the left side of the ionogram in Figure 2.

Only electromagnetic waves within a certain frequency range are reflected by the ionosphere. When the frequency is too low, the D-layer absorption may become prohibitive. When the frequency is above the critical frequency of the F layer, radio waves that are launched vertically pass through the ionosphere and are lost in space. Waves that are launched at lower elevation angles travel a longer trajectory through the ionosphere and are reflected back to earth still. The relationship between the elevation angle and the maximum frequency at which ionospheric radio wave propagation is supported was first formulated by Martyn [29] and is known as the “Secant Law”

$$\text{MUF} = f_v \sec \theta \quad (1)$$

where MUF is the (instantaneous) maximum usable frequency,  $\theta$  is the angle of incidence, and  $f_v$  is the equivalent vertical frequency [21, pp. 157–158], i.e., the highest frequency that is reflected from the ionosphere when launched vertically. This formula, derived for a plane ionosphere, was later corrected for curved earth and ionosphere by Smith [30]. The correction factor is small, typically between 1 and 1.1. As can be seen from this formula, radio waves may be reflected back to earth at a considerable distance, while the area closer to the transmitter, requiring steeper elevation angles, is not covered. This creates an effect typical of ionospheric radio wave propagation, the so-called “Skip Zone”: no signals are received in a ring-shaped area around the transmitter, while outside that ring normal coverage occurs. This is illustrated in Figure 3.

In NVIS, we want to cover a continuous area directly around the transmitter. However, to cover very short distances via the ionosphere, we need to launch radio waves nearly

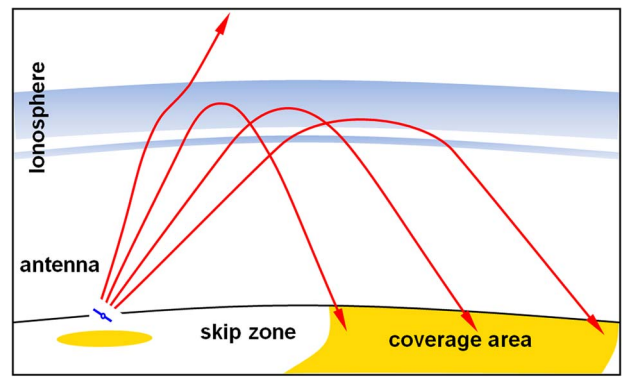


**Figure 3. Ionospheric radio wave propagation above the critical frequency results in a skip zone.**

vertically; therefore, only frequencies below the critical frequency of the intended ionospheric layer can be used. At mid-latitudes in the Northern Hemisphere, good NVIS frequencies typically range from 3 to 10 MHz.

## 2.2 Variability of Ionospheric Propagation

Ionospheric radio wave propagation is highly variable. The electron density profile of the ionosphere, and with it the ionospheric radio wave propagation, differs from location to location and varies with the earth magnetic field, the time of day, and the season. On a longer timescale, it follows the 11-year solar activity cycle, i.e., the “sunspot cycle”, which is shown in Figure 4. Due to the complex and multivariate processes involved, ionospheric radio wave propagation can only be predicted statistically. However, as will be shown in Section 3, a set of specific characteristics for NVIS propagation can still be derived and used for NVIS antenna design. Short-term variability of ionospheric propagation, in terms of minutes, seconds, and milliseconds, makes antenna comparison and hence the verification of a successful antenna optimization by experiment difficult. A solution to this problem will be proposed and demonstrated in Section 5. The influence of the long-term variations on the experiments that are part of our research will be discussed in Section 6.

## 3. NVIS Elevation Angles

To cover very short distances via the ionosphere, radio waves must be launched nearly vertically. For continuous coverage of an area around the transmitter, radio waves must be launched from a certain angle upward, depending on the size of the desired coverage area. Knowledge about these elevation angles is necessary for NVIS antenna optimization.

### 3.1 NVIS Elevation Angle Simulations

To establish the relationship between the radius of NVIS coverage area and the minimum elevation angle, a large number

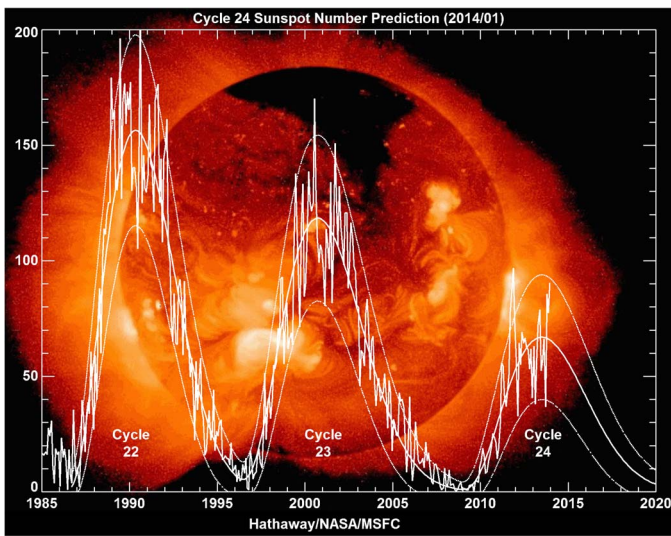


**Figure 4.** Variation of solar activity over three subsequent sunspot cycles. Vertical axis shows the smoothed sunspot number (courtesy: Hathaway/NASA/MSFC).

of simulations were performed using Proplab-Pro [31] version 3, an ionospheric ray tracing program. As the virtual reflection height of the radio waves is frequency dependent, so is the elevation angle. Therefore, several lines are shown Figure 5, each representing the relationship between distance and elevation angle for a specified frequency.

The line colors show the ionospheric layers involved. Red lines show the relationship between elevation angle and distance for frequencies below the critical frequency of the E layer. The radio wave is reflected by the layer regardless of the elevation angle. There is a slight increase in reflection height with increasing frequency, but this does not influence the elevation angle significantly. The blue lines indicate that the frequency of the radio wave is above the critical frequency of the E layer. Low elevation angles are still reflected by the layer, but higher angles pass through it. The waves that pass through are slightly refracted by that passage, after which they are reflected by the F layer. The green lines show waves with sufficiently high frequency to pass through the E layer unaltered, to reflect against the F layer regardless of the elevation angle. At still higher frequencies, the waves are only reflected when launched at low angles.

Two scenarios were examined. One represents a sunspot cycle minimum and is shown in Figure 5; the other represents the maximum of a moderate sunspot cycle (similar to cycle 23 in Figure 4) and is shown in Figure 6. The simulations use the International Reference Ionosphere model version 2007 with the International electron density model of the Committee Consultative on Radiocommunication, the International Geomagnetic Reference Field magnetic field model, and the NeQuick topside model. IG index (effective smoothed sunspot number) is 10 and 120;  $A_p$  and  $K_p$  are set at 0. Transmitter location was  $52^\circ$  N,  $6^\circ$  E; simulation date was set to November 10, 2001, 10:30 UTC. Both simulations use the same date to accentuate the influence of the solar activity

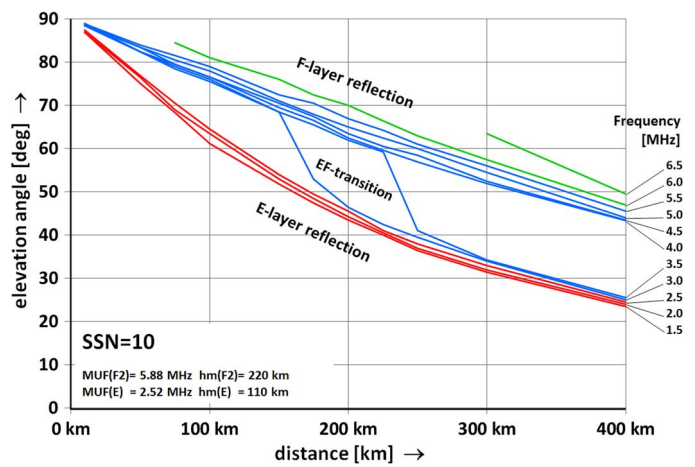


**Figure 5.** Relationship between elevation angle and distance for several frequencies. Simulations for the ordinary wave using Proplab-Pro version 3 [31], for IG index (effective smoothed sunspot number) of 10;  $A_p$  and  $K_p$  are set at 0. These values represent a solar cycle low.

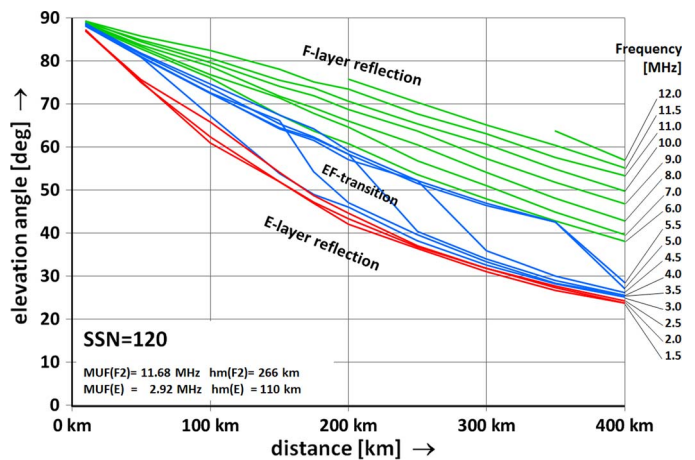


**Figure 6.** Relationship between elevation angle and distance for several frequencies. Simulations for the ordinary wave using Proplab-Pro version 3 [31], for IG index (effective smoothed sunspot number) of 120;  $A_p$  and  $K_p$  are set at 0. These values represent a moderate solar cycle maximum.

alone. Related signal strength levels and absorption are ignored; only the elevation angles for frequencies supported by the ionosphere are examined.

Figure 7 shows the ray paths for a fixed distance at increasing frequencies. The same color coding is used to indicate E-layer reflection (red), E-layer refraction followed by F-layer reflection (blue), and F-layer reflection (green). This figure illustrates that the elevation angle depends not only on the wanted skip distance but also on the operating frequency. Single line graphs, thus ignoring the frequency dependence, for the relationship between elevation angle and skip distance can be found in [21, p. 139]. His curves for E-layer and F-layer reflections correspond with our simulations, but only when frequencies near the MUF are assumed.

Transmitter location is 52° N, 6° E, with a path length of 150 km, in the south direction. IG index is 120; Ap and Kp are set at 0; simulation date is November 10, 2001, 10:30 UTC.

These simulations illustrate that the NVIS elevation angle depends not only on coverage distance but also on the operating frequency and the critical frequency of the E and F layers. Considering the variability of the ionosphere, an all-inclusive relationship between elevation angle and distance cannot be given. However, when we choose an operating frequency that favors F-layer reflection and for a transmitter location at midlatitudes, we can still draw some important conclusions. To realize an NVIS coverage area and with a radius of 150 km, i.e., the size of Switzerland or the State of Louisiana, elevation angles from 68° to 90° for low sunspot numbers or from 65° to 90° for high sunspot numbers seem to be a valid assumption.

### 3.2 NVIS Elevation Angle Measurements

To relate these theoretical findings with practical NVIS propagation properties, elevation angles of 85 NVIS stations were measured at 3.5 MHz and 7 MHz, during a national amateur radio contest. The results were originally published by the authors in amateur radio magazines such as [32]. The measurements were performed on November 10 and 11, 2001, between 08:00 and 11:00 UTC. Over 300 measurements were made, recording azimuth angle and elevation angle. A professional radio direction finder (RDF)-type Rohde & Schwarz (R&S) DDF0xM was used, located 52.24° N, 5.08° E. The RDF consists of nine crossed-loop antennas placed in a 50-m circle, connected to digital receivers followed by correlators. The crossed-loop antennas are fed using a phasing network to provide circular polarization with selectable direction of rotation. During the measurements, the polarization that yielded highest reliability, as indicated by the RDF, was selected. A picture of three of these crossed-loop antennas is shown in Figure 8.

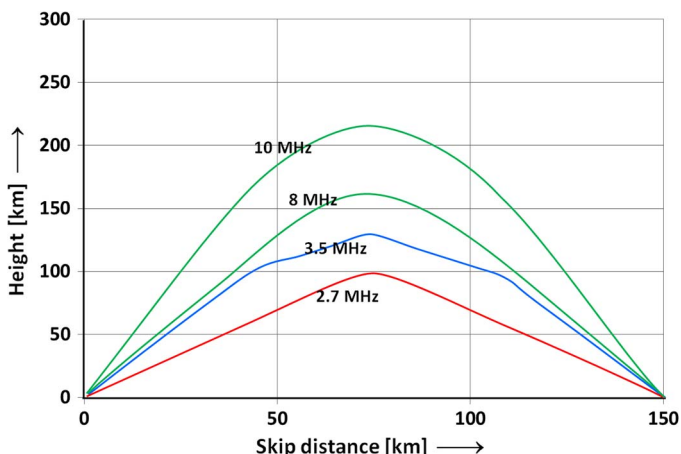


Figure 7. Ionospheric path and corresponding elevation angle for a fixed skip distance for four different frequencies. Proplab-Pro version 3 [31] 2-D ray tracing was used to create this example, and only the ordinary wave paths are shown.

The NVIS stations were spread across the country, at distances ranging from 9 to 165 km. Most NVIS stations used 100-W transmitters and single-wire horizontally polarized antennas. Figure 9 shows the location of these NVIS stations as red dots on the map of The Netherlands. Thin red lines show the azimuth angle and distance from the RDF to each NVIS station. Equidistant circles with 50-km increments are superimposed in gray.

For verification purposes, each radio station was identified by its call sign. Using the address information registered with the call sign, the measured azimuth angle was compared with the expected direction. Where this azimuth angle had a deviation greater than 15°, the station owner was contacted to verify the transmitter location. In most cases, a temporary location was used, which provided a good match with the measured azimuth, and the correct distance was recorded for each measurement. Figures 10 and 11 show the distribution of the measured



Figure 8. Three of the nine crossed-loop antennas of the R&S DDF0xM RDF.



Figure 9. Azimuth and distance from the RDF to the 85 NVIS stations.

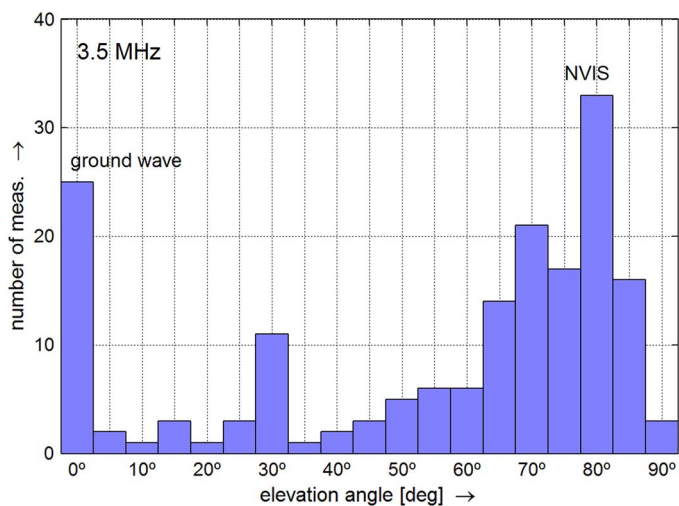


Figure 10. Histogram of measured elevation angles at 3.5 MHz.

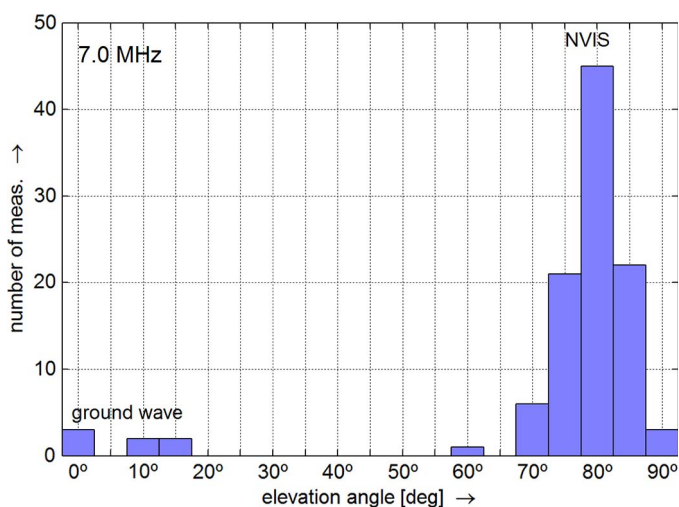


Figure 11. Histogram of measured elevation angles at 7.0 MHz.

elevation angle for these 300 measurements at 3.5 MHz and 7 MHz, respectively.

Measurements with approximately  $0^\circ$  elevation angle indicate arrival via ground wave propagation; the elevation angles above  $70^\circ$  are NVIS. The high proportion of high-angle measurements shows the dominance of NVIS propagation over ground wave. This was very significant at 7.0 MHz, where even radio stations located just 20 km away could only be received via NVIS. According to theory, the ground wave reaches farther on lower frequencies, which explains the higher proportion of ground wave measurements at 3.5 MHz. Figures 12 and 13 show the measured elevation angle as a function of the distance.

The measurements at 3.5 MHz show a large spreading. This may have three reasons. First, the accuracy of the RDF is lower at 3.5 MHz because its physical dimensions are smaller compared with the wavelength. Second, the RDF may have more difficulty in resolving the mix of ground wave and

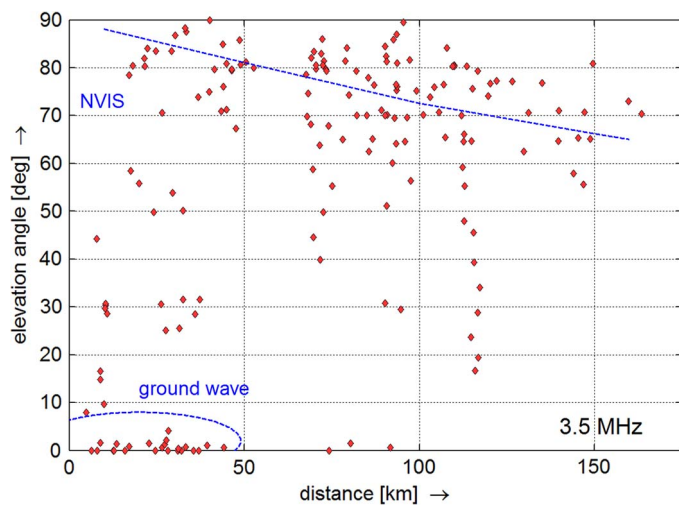


Figure 12. Measured elevation angle versus distance at 3.5 MHz. The blue dashed line shows the expected value, taken from Figure 5.

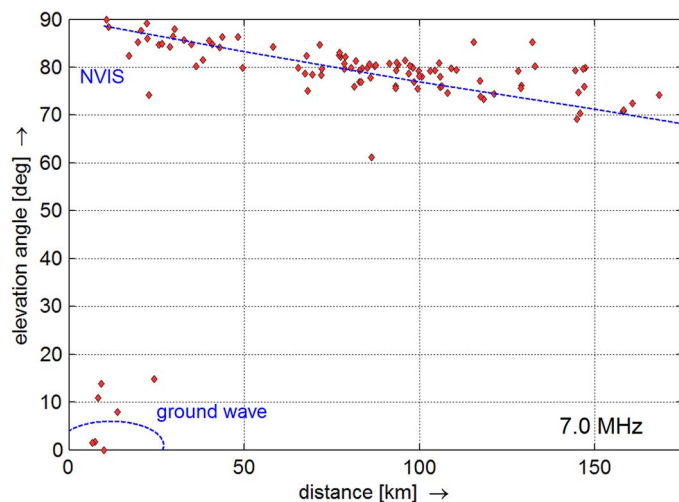


Figure 13. Measured elevation angle versus distance at 7.0 MHz. The blue dashed line shows the expected value, taken from Figure 5.

skywave components at short distances. Finally, due to the lower frequency, both E-layer and F-layer reflections may have occurred within the 3-h measurement interval. As these graphs show, NVIS is dominant over ground wave propagation at distances greater than approximately 40 km at 3.5 MHz, and greater than 20 km at 7 MHz. The measured elevation angles for NVIS coverage from 0 to 165 km range from  $65^\circ$  to  $90^\circ$  at 3.5 MHz, and from  $70^\circ$  to  $90^\circ$  at 7 MHz.

#### 4. NVIS Antenna Optimization

The properties of the employed transmit and receive antennas must match the intended propagation mechanism and

suppress unwanted propagation. For NVIS, this means that an antenna must be selected with a vertical radiation pattern favoring the high elevation angles found through simulation and measurement in Section 3, while suppressing radiation at lower elevation angles. Matching the polarization of the transmit and receive antennas to the propagation mechanism is not considered in this paper, but is discussed in [33].

A wide range of antennas types is available for shortwave applications, each with its specific properties concerning radiation pattern, gain, efficiency, gain bandwidth, impedance bandwidth, and polarization. However, due to the long wavelength, antennas for the intended frequency range will be large. For mobile applications, small loop antennas are popular. For ad-hoc field operations, larger wire antennas strung between existing structures or portable masts provide higher antenna gain and more bandwidth. In addition, arrays can be formed of multiple identical antenna elements to produce an enhanced radiation pattern [34, pp. 127–130]. Antenna arrays for transmission are large and require multiple supports, complex power splitting networks, and phase lines. Receive antenna arrays, on the other hand, may be composed of a number of small low-weight active antennas with much simpler low-power splitters and phasing harness. Such an antenna array can be deployed quickly for base stations in ad-hoc operations. Modern high-end HF radio transceivers supporting the use of separate transmit and receive antennas could be used in emergency base stations. At midlatitudes, if a receive antenna with circular polarization is used, the selection of the ordinary or the extraordinary wave may reduce dispersion and fading. Simultaneous reception of left-hand and right-hand circular polarization can be used for diversity reception. Circular polarization for NVIS can be achieved with two perpendicular horizontally polarized (dipole) antennas fed with  $90^\circ$  phase difference [33]. As this antenna requires only one support, it may even be practical in temporary or ad-hoc installations.

#### 4.1 Influence of Antenna Height

The NVIS propagation mechanism restricts the use of frequencies to the range of approximately 3–10 MHz, corresponding to wavelengths of 30–100 m. NVIS antennas are, therefore, large and often basic antenna types realized as wire antennas strung at low heights, in terms of wavelengths, above ground. As a consequence, NVIS antenna designers must consider the influence of ground proximity: ground absorption and beamforming due to ground reflection. To analyze the effect of antenna height on ground losses and ground reflection gain, a large number of half-wave wire dipoles were modeled at different heights and above different soil types at 5.39 MHz. Numerical Electromagnetics Code (NEC) 4.1 was used, which is a method-of-moments antenna simulation software created at Lawrence Livermore National Laboratories [35]. It includes a Sommerfeld–Norton ground model for realistic simulation of ground reflection and ground loss [36]. A wire radius of 1 mm was assumed. Both the wire radius and the ground proximity influence the resonant length of the antenna. Therefore, in each

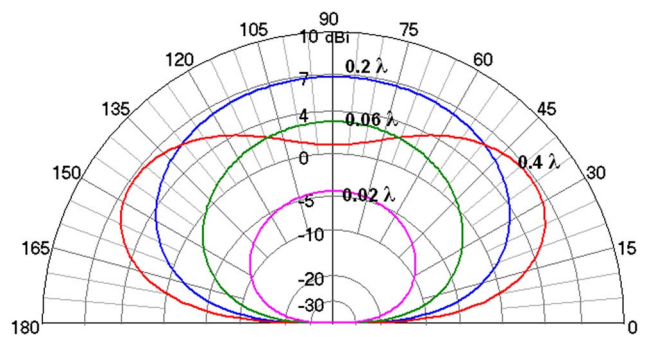


**Figure 14. Vertical radiation pattern of a horizontal half-wave dipole antenna  $0.02\lambda$ ,  $0.06\lambda$ ,  $0.20\lambda$ , and  $0.40\lambda$  above farmland soil at 5.39 MHz. Intensity axis shows antenna gain in decibels over an isotropic radiator (dBi).**

simulation, the antenna length was corrected to achieve resonance. A selection of the simulations is shown in Figure 14, illustrating the influence of increasing antenna height on the antenna gain and the vertical radiation pattern of horizontal half-wave dipoles above farmland soil ( $\sigma \approx 20$  mS/m,  $\epsilon_r \approx 17$ ).

When the antenna is mounted at a very low height ( $0.02\lambda$ ), the antenna gain is low. The antenna diagram shows considerable directivity, but a substantial portion of the transmit power is lost in the ground underneath the antenna. With increasing antenna height ( $0.06\lambda$ ), the amount of beamforming due to ground reflection decreases slowly, and the antenna directivity decreases. However, the ground losses decrease much faster, so that the resulting antenna gain increases, until maximum antenna gain is realized around  $0.2\lambda$ . When the antenna height is further increased (in our example to  $0.4\lambda$ ), the radiation pattern flattens and the maximum antenna gain occurs at lower elevation angles. At the elevation angles needed for NVIS, however, the antenna gain decreases. This process continues until, at  $0.5\lambda$ , a minimum is found at  $90^\circ$  elevation angle. At heights above  $0.5\lambda$ , the high-angle radiation starts to increase again, but now sidelobes at lower elevation angles are created, which we consider undesirable because of the increasing interference to and from other stations located farther away.

#### 4.2 Simulated Optimum NVIS Transmit Antenna Height

Normally, antenna gain is defined in the direction of maximum radiation. This definition cannot be used in NVIS research, as Figure 14 illustrates: with the antenna mounted at  $0.4\lambda$  above ground, the maximum gain occurs at an elevation angle of  $35^\circ$ , while the antenna gain at NVIS elevation angles is much lower. To produce the highest field strength in the coverage area, the radiated power has to be directed toward the high elevation angles used in NVIS. Therefore, to be used in our optimization, we introduce “NVIS Antenna Gain” ( $G_{\text{NVIS}}$ ), as the average antenna gain at NVIS elevation angles, i.e., between  $70^\circ$  and  $90^\circ$  for a coverage area with a radius of 150 km. Another elevation angle range can be chosen if a larger NVIS coverage area is targeted. That is

$$G_{\text{NVIS}} = \frac{\int_{\varphi=0}^{2\pi} \int_{\theta=0}^{\frac{\pi}{9}} G(\theta, \varphi) \sin \theta d\theta d\varphi}{\int_{\varphi=0}^{2\pi} \int_{\theta=0}^{\frac{\pi}{9}} 1 \sin \theta d\theta d\varphi} = \frac{\int_{\varphi=0}^{2\pi} \int_{\theta=0}^{\frac{\pi}{9}} G(\theta, \varphi) \sin \theta d\theta d\varphi}{2\pi(1 - \cos \frac{\pi}{9})} \quad (2)$$

where  $\varphi$  is the azimuth angle, and  $\theta$  is the zenith angle, both expressed in radians, and  $G(\theta, \varphi)$  is the antenna gain in the direction  $(\theta, \varphi)$ , expressed as a linear value. Elevation angles of  $70^\circ$ – $90^\circ$  correspond with zenith angles of  $0^\circ$ – $20^\circ$  or  $0$  to  $\pi/9$  radians.

In analogy, “NVIS Directivity” ( $D_{\text{NVIS}}$ ) is defined as the average directivity for elevation angles between  $70^\circ$  and  $90^\circ$ , as follows:

$$D_{\text{NVIS}} = \frac{\int_{\varphi=0}^{2\pi} \int_{\theta=0}^{\frac{\pi}{9}} D(\theta, \varphi) \sin \theta d\theta d\varphi}{2\pi(1 - \cos \frac{\pi}{9})} \quad (3)$$

where  $D(\theta, \varphi)$  is the directivity in the direction  $(\theta, \varphi)$ , i.e., the antenna gain in that direction divided by the average antenna gain over all possible spatial angles, expressed as a linear value. The output of the NEC 4.1 simulations is now reprocessed using (2) and (3). Figure 15 shows  $G_{\text{NVIS}}$  and  $D_{\text{NVIS}}$  as a function of the antenna height for farmland soil. It can be seen that, for farmland, the NVIS directivity varies only slowly with height with an optimum  $h_{\text{RX}}$  at  $0.09\lambda$ , whereas the NVIS Antenna Gain has a distinct optimum  $h_{\text{TX}}$  at  $0.19\lambda$  and sharply decreasing at low heights due to excessive ground loss. The NVIS Antenna Gain is 11.3 dB lower at  $0.02\lambda$ .

Figure 16 compares the NVIS antenna gain for several ground types. The optimum NVIS transmit antenna height lies between  $0.18\lambda$  and  $0.22\lambda$  for most ground types. Above sea water, the optimum height is  $0.13\lambda$ . Higher ground conductivity and higher permittivity result in higher NVIS antenna gain, with 2.2 dB increase from urban soil to clay soil and another 1.1 dB from clay soil to sea water. The optimum NVIS transmit antenna heights ( $h_{\text{TX}}$ ) found for several soil types are summarized in Table 1. For completeness it must be noted that some freshwater lakes show conductivities of up to 50 mS/m due to (industrial) pollutants. This increases the antenna gain by 2–3 dB from the values found for freshwater lakes for an antenna height of  $0.02\lambda$ . The effect is less for greater heights. In that case, the optimum height will be close to that of clay ground.

### 4.3 Simulated Optimum NVIS Receive Antenna Height

Optimization of the receive antenna height is similar to that of the transmit antenna but not identical. On the receive

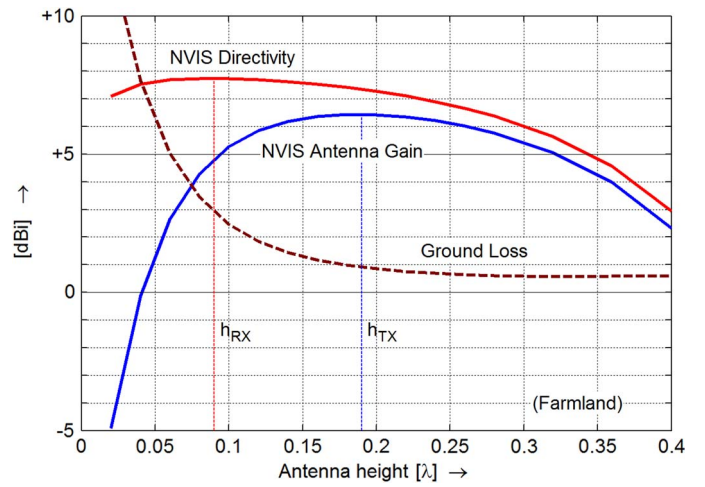


Figure 15. NVIS antenna gain (blue) and directivity (red) of a horizontal half-wave dipole antenna versus height above farmland soil at 5.39 MHz. Ground loss in decibels.

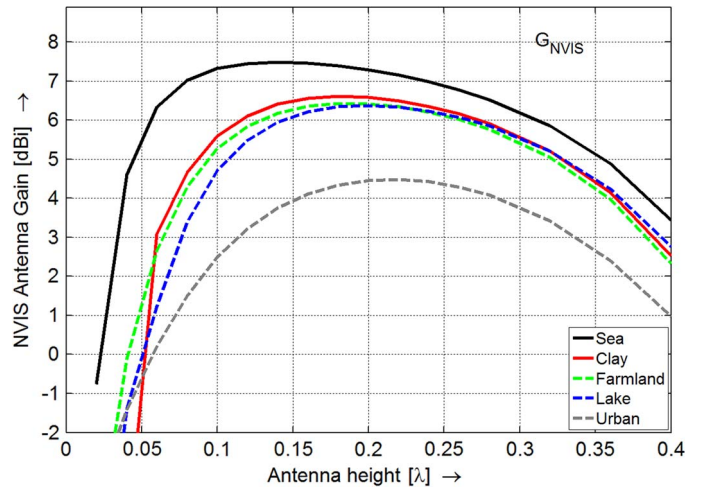


Figure 16. NVIS antenna gain ( $G_{\text{NVIS}}$ ) of a horizontal half-wave dipole antenna versus height for several soil types at 5.39 MHz. NVIS antenna gain is the average antenna gain for NVIS elevation angles, here between  $70^\circ$  and  $90^\circ$  for a coverage area with a radius of 150 km.

Table 1. Optimum NVIS transmit antenna height ( $h_{\text{TX}}$ ), i.e., the height above ground for a horizontal half-wave dipole antenna that yields the highest NVIS gain, for several soil types.

Soil type	$\sigma$	$\epsilon_r$	$h_{\text{TX}}$
Urban	1 mS/m	5	$0.22\lambda$
Lake*	5 mS/m	80	$0.20\lambda$
Farmland	20 mS/m	17	$0.19\lambda$
Clay	30 mS/m	20	$0.18\lambda$
Sea	5000 mS/m	80	$0.13\lambda$

\* Some rivers and fresh water lakes show conductivities of 50 mS/m or more due to the presence of (industrial) pollutants.

side, the reception threshold is determined by SNR, rather than signal strength [34, p. 766]. Hence, the antenna must be selected for the highest discrimination between NVIS signals and unwanted signals arriving from other directions, and for the lowest susceptibility to natural and man-made ambient noise, which may arrive via skywave or via line of sight. As the origin of the interference and the ambient noise is not known *a priori*, all azimuth and elevation angles are considered equally likely to produce interference and noise. Likewise, if the exact location of the NVIS signal source within the coverage area is not known, the best approximation is to use the average antenna gain calculated over the corresponding elevation angles for the wanted signal. With these assumptions, the discrimination factor (DF) is equal to the division of the average antenna gain over the NVIS elevation angles and the average gain over all possible elevation angles and corresponds with the NVIS directivity. That is

$$DF = \frac{\int_{\varphi=0}^{2\pi} \int_{\theta=0}^{\frac{\pi}{9}} G(\theta, \varphi) \sin \theta d\theta d\varphi}{\int_{\varphi=0}^{2\pi} \int_{\theta=0}^{\frac{\pi}{9}} 1 \sin \theta d\theta d\varphi} \bigg/ \frac{\int_{\varphi=0}^{2\pi} \int_{\theta=0}^{\pi} G(\theta, \varphi) \sin \theta d\theta d\varphi}{\int_{\varphi=0}^{2\pi} \int_{\theta=0}^{\pi} 1 \sin \theta d\theta d\varphi} = \frac{G_{\text{NVIS}}}{\eta} = D_{\text{NVIS}}. \quad (4)$$

This implies that, on reception, NVIS directivity must be optimized rather than NVIS antenna gain. The ground reflection still influences the vertical radiation pattern and contributes to NVIS directivity, but lower antenna efficiency due to ground loss no longer plays a role, as both wanted and unwanted signals suffer the same loss. That is: as long as the receiver noise figure is low enough, so that the ambient noise determines the reception threshold.

To calculate the theoretical maximum NVIS directivity that can be realized, let us consider a perfect conical beam toward the zenith with  $40^\circ$  beam width, with a uniform sensitivity over the elevation angles from  $70^\circ$  to  $90^\circ$  and no response at all at other elevation angles. The directivity of such an idealized antenna can be calculated as

$$D_{\text{NVIS,max}} = \frac{4\pi}{\int_{\varphi=0}^{2\pi} \int_{\theta=0}^{\frac{\pi}{9}} 1 \sin \theta d\theta d\varphi} = \frac{4\pi}{2\pi(1 - \cos \frac{\pi}{9})} \approx 33.16 \quad (5)$$

The maximum achievable  $D_{\text{NVIS}}$  is  $10 \log_{10}(33.16) = 15.2$  dBi. If a uniform distribution of the ambient noise is assumed, the SNR of such an antenna would also be 15.2 dB higher, which is substantial. Most practical implementations will not achieve such values, although an array of active receive antennas employing digital beamforming may approach this value [37].

To analyze the influence of the receive antenna height, NVIS directivity is plotted against antenna height for different ground types in Figure 17. The optimum NVIS receive antenna

heights ( $h_{\text{RX}}$ ) found for several soil types are summarized in Table 2. The receive antenna height seems not critical: the variation in NVIS directivity is only 0.8 dB over a range from  $0.02\lambda$  to  $0.22\lambda$ . In addition, the difference between the various soil types is small, i.e., less than 1 dB.

## 5. Comparison of HF Antenna Performance in the Presence of Fading

The optimum antenna heights are found through simulation and therefore require empirical verification. However, to obtain an accurate and reproducible antenna gain and antenna SNR comparison at HF is challenging. Ionospheric radio wave propagation, including NVIS, is subject to signal fading caused by changing properties of the ionosphere and by interference of waves traveling different paths through the ionosphere (multipath fading).

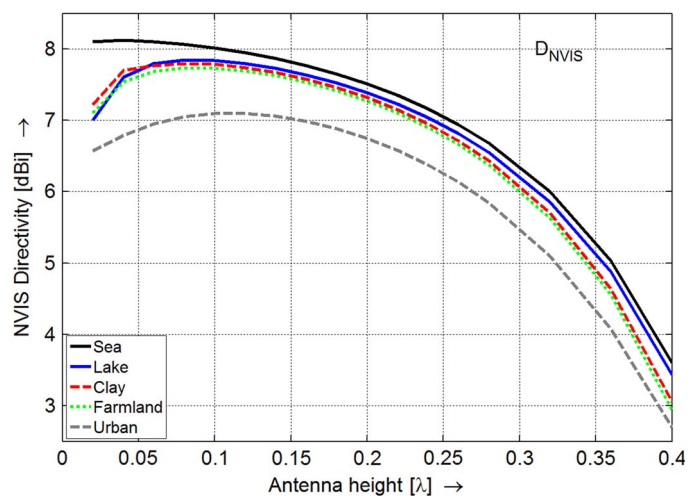


**Figure 17. NVIS directivity ( $D_{\text{NVIS}}$ ) of a horizontal half-wave dipole antenna versus height for several soil types at 5.39 MHz. NVIS directivity is the average directivity for NVIS elevation angles, here between  $70^\circ$  and  $90^\circ$  for a coverage area with a radius of 150 km.**

**Table 2. Optimum NVIS receive antenna height ( $h_{\text{RX}}$ ), i.e., the height above ground for a horizontal half-wave dipole antenna that yields the highest NVIS directivity, for several soil types.**

Soil type	$\sigma$	$\epsilon_r$	$h_{\text{RX}}$
Urban	1 mS/m	5	$0.11\lambda$
Lake*	5 mS/m	80	$0.09\lambda$
Farmland	20 mS/m	17	$0.09\lambda$
Clay	30 mS/m	20	$0.08\lambda$
Sea	5000 mS/m	80	$0.04\lambda$

\* Some rivers and fresh water lakes show conductivities of 50 mS/m or more due to the presence of (industrial) pollutants.

The signal may experience fast multipath fading with an interval time of 2–6 s and notches varying in depth between 10 and 30 dB, superimposed on slow fading over an interval of 15–60 s. The channel response, i.e., delay spread and Doppler shift in the first tens of milliseconds, has been subject to a lot of studies, with the improvement of HF data modems in mind [38]. Less literature is available on amplitude fading on a longer timescale [39]. The values mentioned come from practical experience but correspond well with [39] and [40]. Multipath fading may produce a null at one of the antennas, while the other still has maximum signal. As a result of the spatial separation and different radiation patterns of the antennas, the signal variations are not necessarily correlated on each of the antennas that are compared. As a result of this, making only a few short-term signal strength comparisons would result in errors of up to 20 dB. A better solution is proposed in the following.

### 5.1 Proposed New Evaluation Method

The following method, which is designed particularly for the comparison of HF antennas, *in situ* and with real signals and propagation, produces accurate and reproducible results:

A stable beacon transmitter is installed at a sufficient distance from the antenna test site to generate strong NVIS signals and a negligible ground wave component. At the antenna test site, several antennas under test (AUTs) are installed in such a way that coupling between them is minimized. The constitution of the ground under each of the antennas that we compare is (roughly) the same. The AUTs are connected to a measurement receiver through an antenna switch. Both the measurement receiver and the antenna switch are computer controlled. A block diagram can be found in Figure 18. Signal strength and ambient noise level of each AUT are measured sequentially over a long period of stable NVIS propagation. The noise level is measured in the “off” period of the transmitter and on adjacent

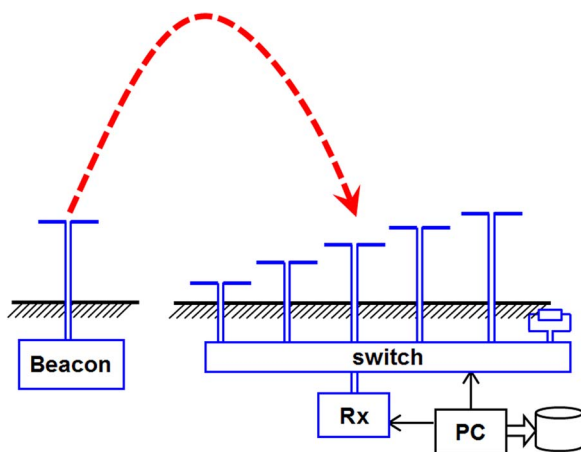


**Figure 18. Block diagram of the proposed setup for the comparison of signal strength and SNR on five antennas mounted at different heights, *in situ* and with real-life signals and propagation. The sixth port is terminated with a 50-Ω load.**

channels. SNR is calculated for each measurement sample. One switch port is terminated in the characteristic impedance of the receiver, so that the receiver noise is also measured as a separate value. The distribution of the measured values of each AUT is plotted in one combined graph. When a large number of measurements are taken, each AUT shows a single-peaked distribution, facilitating comparison of relative signal strength and SNR. This method remains very close to the practical use situation and produces accurate results.

Hagn [15] described a comparable method in 1973, using an ionosonde to send pulses upward toward the zenith. The reflected pulses were received on the AUT and a reference antenna. The receiver was rapidly switched between these two antennas, and the receiver output recorded with an ink paper recorder. A step attenuator was inserted in the feed line of the more efficient antenna and manually adjusted until the signal was equal on both antennas. The attenuator value then represented the antenna gain difference. His method provides relative antenna gain for signals arriving at zenith angles only and represents one single instant. It does not take into account the ionospheric variation over time and does not consider receive SNR.

The new method that is presented here profits from the advances in accuracy of the measurement receivers and the possibility to digitally store large numbers of measurements for postprocessing. The use of a carrier signal, instead of short pulses, simplifies the equipment needed. As the intervals, over which data are collected, are significantly longer than those used in [15], the method presented here can be used to evaluate antenna performance under varying propagation conditions. In addition, both received signal strength and SNR can be evaluated using this method.

Although designed for the verification of the optimum NVIS antenna heights in this investigation, it can easily be adapted for the evaluation of other antennas. When antennas intended for longer propagation paths are compared, the variance will be higher, just as will be the case in the actual application. The method will be excellent for the comparison of the *in situ* performance of two or more antennas.

### 5.2 Practical Realization of the Proposed Method

The implementation of our experiment is described as follows and includes several practical solutions to enhance accuracy. Our experiment took place from April 1, 2009, at 15:27h UTC, to April 2, 2009, at 12:58h UTC, during the sunspot minimum between sunspot cycles 23 and 24, as shown in Figure 4. Consequently, the critical frequency  $f_xF2$  was very low, i.e., below 6.5 MHz. Therefore, to ensure that NVIS propagation was present during a significant part of the measurement period, the experiment was performed at 5.39 MHz. A special permission was obtained for the use of this frequency. The beacon transmitter, constructed by A. J. Westenberg and capable of producing a continuous RF carrier output of 850 W during 24 h, is



**Figure 19. Beacon transmitter, capable of 850-W RF output continuous transmission at 5.39 MHz.**

shown in Figure 19. Transmitter output power stability was better than 0.1 dB over the entire measurement period. The frequency drift was less than 5 Hz (1 ppm). This transmitter was set up near Lucaswolde, The Netherlands (approximately 53.2° N, 6.3° E), feeding a horizontal half-wave dipole at 8.5 m (0.15λ) above clay soil. The simulated antenna gain is 6.3 dBi. This results in 3.6-kW or 35.6-dBW equivalent isotropically radiated power.

Approximately 127 km further to the south, near Eibergen, The Netherlands (approximately 52.1° N, 6.6° E), an open area with farmland soil was available for the installation of five horizontal half-wave dipole antennas. The antenna heights were selected from the previous simulations, so that signal differences between the antennas were expected to be discernible. Chosen heights were 0.02λ, 0.05λ, 0.09λ, 0.16λ, and 0.22λ. For 5.39 MHz, this corresponds with 3, 5, 9, and 12.5 m. Each antenna was adjusted for resonance after installation, to compensate for detuning due to ground proximity. Mutual coupling between the antennas was reduced by installing them end to end and in a straight line, as shown in Figure 20. Additionally, each antenna was connected to the antenna switch with a feed line of which the length was cut to an odd multiple of electrical quarter wavelengths. When not selected, the feed line was shorted by the switch. This short circuit transforms to a high impedance at the center of the dipole, effectively splitting it into two nonresonant halves. Figure 21 shows the calibrated professional



**Figure 20. Three of the five AUTs.**

measurement receiver R&S FSMR26 used for our measurements. For absolute values, the combined measurement uncertainty is 0.3 dB for 95% confidence [41].

Measurements at HF put high demands on receiver linearity due to the presence of strong broadcast signals. To verify that the measurement receiver was operated within its intermodulation-free dynamic range, the total power present at the antenna input was measured over 24 h using a 20-MHz wide IF filter. Based on the results of this measurement, a bandpass filter was built and inserted at the receiver input to prevent overloading by strong out-of-band signals. The transmitter and receiver drift was below 5 Hz over a 24-h interval. This, and the use of carrier (continuous wave) transmissions instead of the pulsed transmissions used by Hagn [15], made measurements using a 30-Hz IF filter possible, which provided high immunity to in-band interference. The measurements were automated using a custom measurement program written in LabView. The frequency was held free for the experiments. Even so, a series of 30-Hz frequency bins was measured around the receive frequency, so that a spectrogram was obtained, which was used to monitor for any unexpected interfering signal that could compromise the measurements. The transmitter carrier was switched on and off in a precisely timed slow (1-min) on/off cycle, synchronized to the DCF-77 time signal transmitter. This made identification easy and enabled observation of interference and noise measurement on the transmit frequency. As the spectrogram in Figure 22 shows, no interference was present on or near the measurement frequency.

### 5.3 Empirical Verification of the Optimum NVIS Transmit Antenna Height

Using the setup described in Section 5.2, measurements were started at 15:27h UTC and continued through 12:58h the next day. Within this time span, stable F-layer NVIS propagation was present during two intervals: from 15:27h to 19:05h and from 09:40h to 12:58h UTC. Figure 23 shows the received signal strength over time, and both intervals are marked NVIS

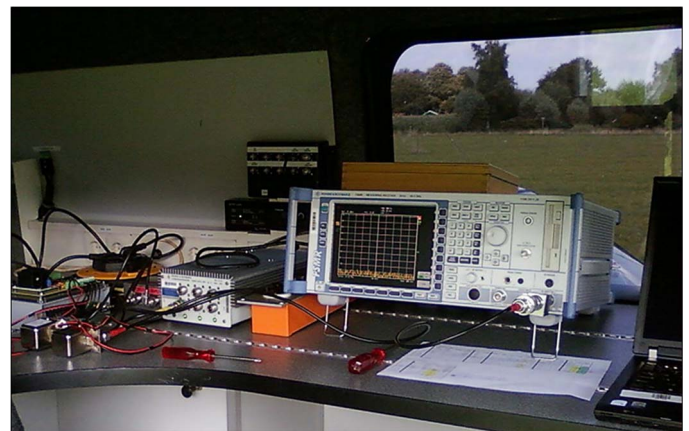


**Figure 21. R&S FSMR26 measurement receiver with coaxial switches and LabView automation.**

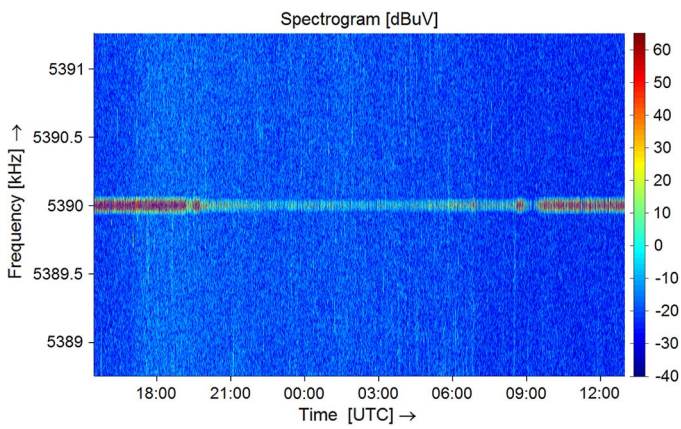


**Figure 22. Spectrogram of the beacon and adjacent frequencies on one of the AUTs.**

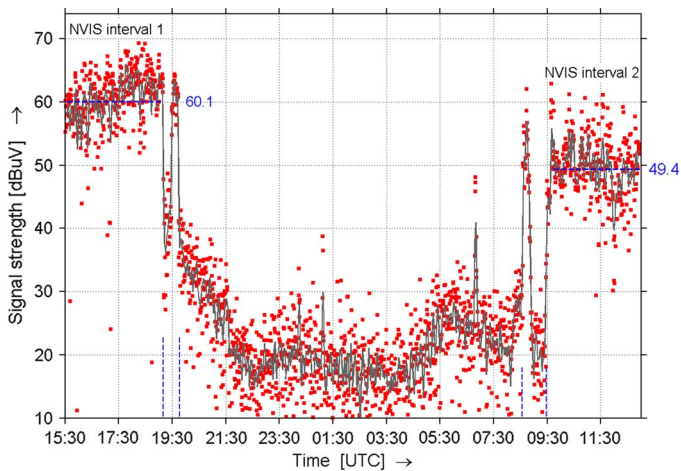


**Figure 23. Signal strength versus time on one of the AUTs. Both NVIS intervals are indicated. A gray line shows the 8-min floating average. The blue vertical dashed lines show the interval in which the NVIS propagation switches between “on” and “off”.**

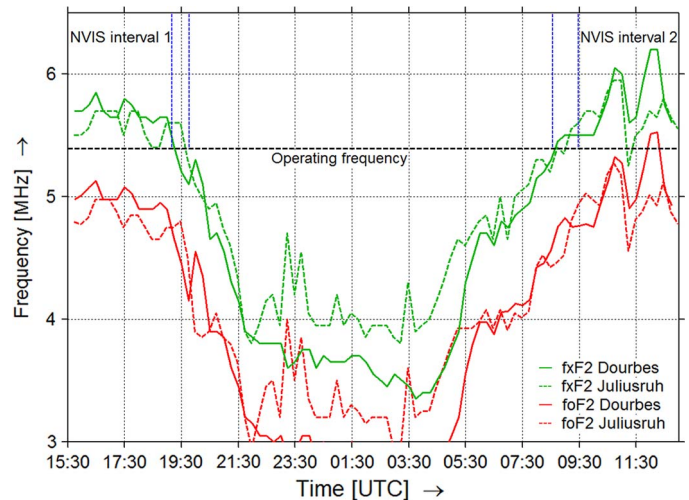
intervals 1 and 2. The blue dashed vertical lines mark the interval in which the NVIS propagation switches from “on” to “off”, in this particular case with some “hesitation”. This “hesitation” is caused by the short-term variation of  $fxF2$  around the value needed to support NVIS propagation. In between NVIS intervals 1 and 2, we had expected to observe no signal at all, or just a weak ground wave signal with slight variance. Instead, the signal remained clearly readable and measurable, far above the ambient noise, and it had all the properties of a skywave signal (fast fading and flutter).

Figure 24 shows the measured  $foF2$  (red) and  $fxF2$  (green). Solid and dashed lines represent data from the Dourbes ionosonde and Juliusruh ionosonde, respectively. As can be seen, NVIS propagation is possible when  $fxF2$  exceeds the operating frequency. This conforms to theory [20, 26].

The measurements of NVIS intervals 1 and 2 are processed separately, as the measured average signal level in the morning

is about 12 dB lower than in the evening. The distributions of the signal strength on each antenna are shown in Figure 25 (first NVIS interval) and Figure 26 (second NVIS interval).

For each interval, the total number of samples per antenna is 700; histogram resolution is 0.1 dB. The measurement uncertainty of the receiver (R&S FSMR26) for this frequency range is 0.3 dB ( $2\sigma$ ) for absolute values. As we compare antennas, the systematic error falls out of the equation, and the measurement uncertainty is better than 0.2 dB ( $2\sigma$ ). The measurement resolution is much smaller still (0.01 dB), and 66% of the measurements fall in a 0.1-dB window around the true value. Slight smoothing is applied using a sliding Gaussian window ( $\sigma = 0.15$  dB,  $N = 41$ ). The smoothing parameters chosen are a compromise between resolution and smoothness of the curve.



**Figure 24. Measured  $foF2$  (red) and  $fxF2$  (green) over time. Solid lines represent data from the Dourbes ionosonde and dashed lines from the Juliusruh ionosonde. The blue vertical dashed lines show the interval in which the NVIS propagation switches between “on” and “off”.**

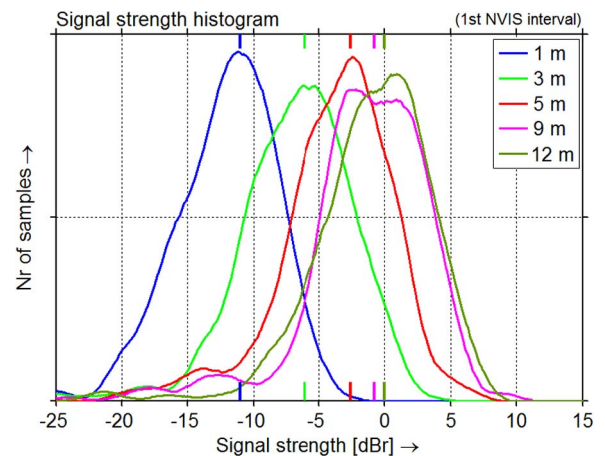


**Figure 25. Histogram of the signal strength on five identical antennas mounted at different heights, first NVIS interval. 0 dBr  $\equiv$  61.5 dB $\mu$ V.**

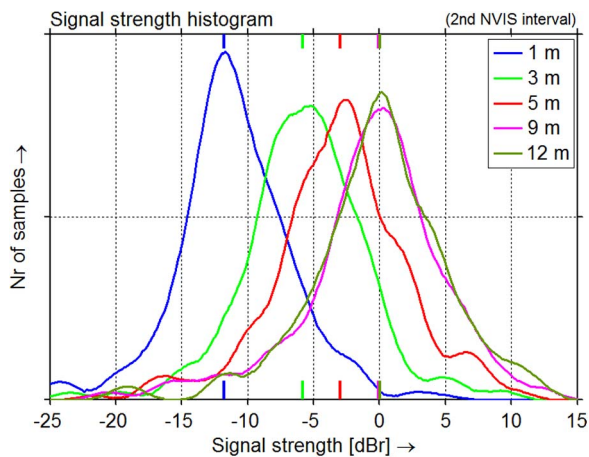


**Figure 26. Histogram of the signal strength on five identical antennas mounted at different heights, second NVIS interval. 0 dBr  $\equiv$  49.5 dB $\mu$ V.**

The mean values of the measurements are marked in the graphs, and their values are summarized in Table 3. The expected values that were derived from the simulations in Section 4. 2 and shown in Figure 16 and Table 1 are added for comparison. The signal strength measurements closely match the NVIS antenna gain values found by simulation.

### 5.4 Empirical Verification of the Optimum NVIS Receive Antenna Height

On each of the antennas, we measured both signal strength and ambient noise level to calculate SNR. This is done as follows.

During the measurements, the received noise was measured in the 1-min intervals that the transmitter was off, but also continuously in the adjacent frequency bins (30-Hz channels).

The ambient noise can only be measured correctly if the receiver noise floor is low enough. The noise contribution of the receiver itself was measured on the sixth port of the antenna switch, which was terminated with a 50- $\Omega$  load, as shown in Figure 18. Throughout the experiment, the measured noise power was 7–20 dB higher than the receiver noise floor on the highest antenna, and 3–11 dB on the lowest antenna. The latter, representing the worst case, is shown in Figure 27. The true

**Table 3. Comparison of expected and measured NVIS antenna gain for a dipole antenna above farmland soil.**

Antenna height		NVIS Antenna Gain		
		Expected	Meas.1	Meas.2
12.5 m	$0.22\lambda$	-0.2 dBr	0.0 dBr	0.0 dBr
9 m	$0.16\lambda$	-0.0 dBr	-0.8 dBr	0.0 dBr
5 m	$0.09\lambda$	-1.5 dBr	-2.6 dBr	-3.0 dBr
3 m	$0.05\lambda$	-5.0 dBr	-6.1 dBr	-5.8 dBr
1 m	$0.02\lambda$	-12.0 dBr	-11.0 dBr	-11.8 dBr

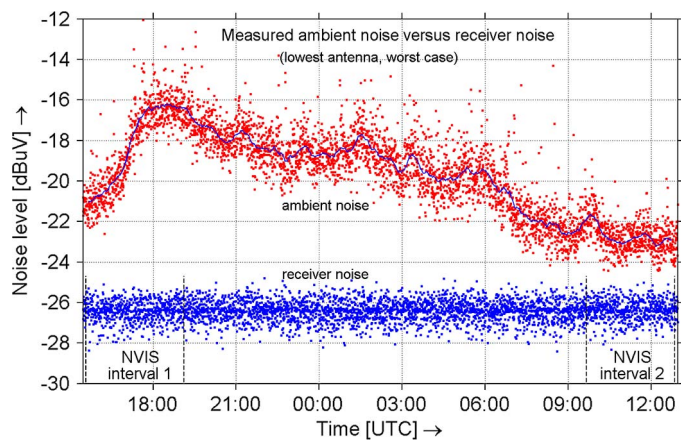


**Figure 27. Measured ambient noise on the lowest AUTs (worst case) versus time, shown as red pixels, with superimposed 12-min average. The blue pixels show the receiver noise.**

value of the ambient noise was calculated from the measured ambient noise and the measured receiver noise on a sample-by-sample basis and used in the subsequent analysis.

The measured ambient noise samples and the measured signal strength samples were used to calculate the SNR per sample. These values were then processed in the same way as has been done for the received signal strength samples in the previous paragraph.

Again, the measurements for both NVIS intervals, from 15:27h to 19:05h and from 09:40h to 12:58h UTC, are processed separately. The distributions of the SNR on each antenna are shown in Figures 28 and 29. For each interval, the total number of samples per antenna is 700; histogram resolution is 0.1 dB. Slight smoothing is applied using a sliding Gaussian window ( $\sigma = 1.3$  dB,  $N = 41$ ). Again, the smoothing parameters chosen are a compromise between resolution and smoothness of the curve.

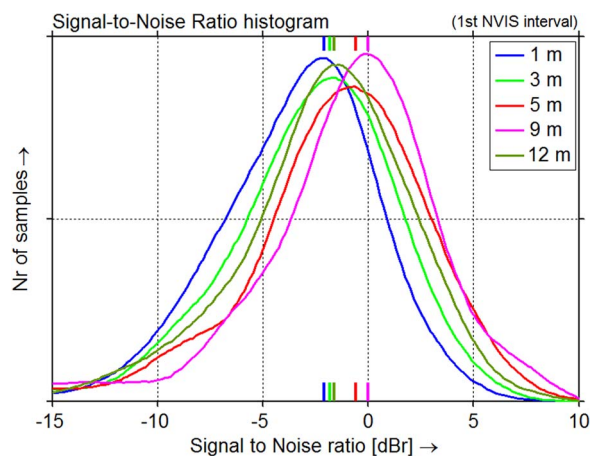


**Figure 28. Histogram of the SNR on 5 identical antennas mounted at different heights, first NVIS interval. 0 dBr  $\equiv$  71.9-dB SNR.**

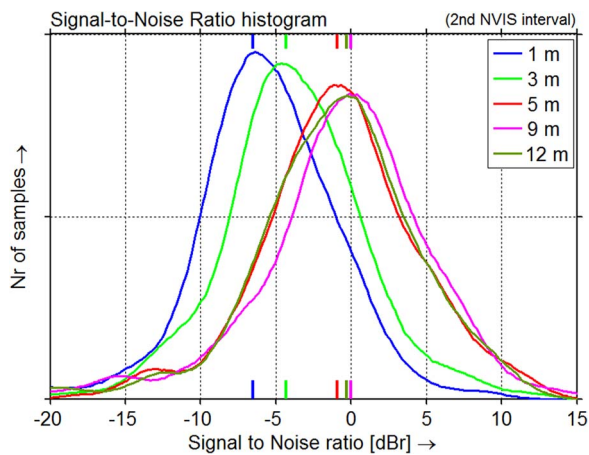


**Figure 29. Histogram of the SNR on five identical antennas mounted at different heights, second NVIS interval. 0 dBr  $\equiv$  69.3-dB SNR.**

The mean values of the measurements are marked in the graphs, and their values are summarized in Table 4. The NVIS directivity values derived from the simulations in Section 4.3 and shown in Figure 16 and Table 2 are added for comparison. When a uniform spatial distribution of the ambient noise is assumed, a direct relationship between the two is expected. However, as Table 4 shows, the optimum NVIS receive antenna height found empirically is slightly higher than the simulation suggested: around  $0.16\lambda$  instead of  $0.09\lambda$ . In addition, the measured SNR values decrease faster with decreasing antenna height than was expected from the simulations.

The theoretical optima were obtained, assuming uniform spatial distribution of the ambient noise, as no *a priori* knowledge is available about the azimuthal direction and elevation angle from which natural noise and man-made noise would arrive at an ad-hoc receive site. When, however, a large number of man-made noise sources arrive via skywave, e.g., from a city or an industrial area, specific spatial directions will contribute more noise than others. In addition, if a few dominant man-made noise sources are present at close range, their signals will arrive via ground wave and from specific angles. This has not been considered in the simulations and could possibly explain the difference between the measured and simulated optima.

**Table 4. Comparison of expected and measured NVIS SNR for a dipole antenna above farmland soil.**

Antenna height		NVIS SNR		
		Expected	Meas.1	Meas.2
12.5 m	$0.22\lambda$	-0.8 dBr	-1.6 dBr	-0.3 dBr
9 m	$0.16\lambda$	-0.2 dBr	0.0 dBr	0.0 dBr
5 m	$0.09\lambda$	0.0 dBr	-0.6 dBr	-0.9 dBr
3 m	$0.05\lambda$	-0.3 dBr	-1.8 dBr	-4.3 dBr
1 m	$0.02\lambda$	-0.8 dBr	-2.1 dBr	-6.5 dBr

## 6. Analysis and Discussion

The research described in this paper was performed at 5.39 MHz, on one location and one instant within the solar cycle. A coverage area size of 150 km was presumed. This section discusses the applicability for other scenarios.

### 6.1 Sensitivity to Frequency and Coverage Area Size

All simulations in Section 4 were done at 5.39 MHz. To assess the influence of the operating frequency, additional simulations were done at 3 MHz and 15 MHz for all soil types specified in Tables 1 and 2. The effect on directivity over this frequency range is smaller than 0.5 dB for all heights and soil types. The absolute antenna gain decreases by 0.1 to 2 dB for a frequency change from 3 to 15 MHz, but the optimum heights are not significantly changed.

The optima found in Section 4 are for NVIS elevation angles between  $70^\circ$  and  $90^\circ$ , targeting a coverage area with a radius of 150 km. If a larger area is targeted, this optimum height will be slightly higher. Increasing height will result in lowering of the elevation angle at the cost of reduction in antenna gain for higher elevation angles. As  $D_{\text{NVIS}}$  and  $G_{\text{NVIS}}$  are the average gain and directivity over a range of elevation angles, the effect is not very sensitive to small changes in coverage area. For much larger areas, however, e.g., to a radius of 500 km, the influence will be more notable, and the procedure described in Sections 3.1 and 4.2 and 4.3 can be followed to find the applicable optima.

### 6.2 Influence of Solar Activity

As the measurements were carried during one day during a sunspot minimum, this raises the question on the applicability of the results to other parts of the solar cycle. First of all, the elevation angles will vary with the sunspot number, as was shown in Figures 5 and 6. However, the variation is not important for NVIS aiming as long as a frequency is chosen favoring F-layer propagation.

The verification measurements are performed during a solar cycle minimum, and low sunspot activity obliges all shortwave users to use lower frequencies. This generally results in congestion in the lower part of the shortwave during sunspot minima, which would result in the “worst case” situation considering interference. However, this aspect has no influence on the measured SNR values, as they are all measured in a clear channel. Optimized NVIS directivity will of course also provide the lowest susceptibility to interference of non-NVIS radio signals, i.e., interference signals arriving via lower elevation angles, but this has not been measured. It is true that ambient noise distributions may be different around the sunspot maximum than at the sunspot minimum, but this has not been researched.

## 6.3 Comparison With Other Research

Austin [42] used simple formula using geometric optics to relate antenna height to the elevation angle at which maximum radiation occurs. He starts assuming perfect conducting ground underneath the antenna and arrives at an optimum height of  $\lambda/4$  for perfect conducting ground, as was expected. He then modifies his formula with an empirical correction factor, derived from NEC computations over rural ground ( $\sigma \approx 5$  mS/m,  $\epsilon_r \approx 13$ ). He then arrives at an optimum height of  $0.22\lambda$  for NVIS angles, which corresponds very well with the values found here. Austin states that “this particular result is not overly sensitive to ground conductivity changes by an order of magnitude. It is somewhat more sensitive to a change in relative permittivity and also more so at lower frequencies,” but does not substantiate this statement with calculations or experiments.

Extensive military research was performed by Barker *et al.* [13] in several terrain and vegetation types. They state in the abstract that “. . .that the effect of the antenna height is the most significant variable” influencing the radiation patterns. Their research focused on the antenna gain at zenith angle, not the average antenna gain over all NVIS angles. However, in Figs. 37 and 41 of their report [13], they show antenna gain values that are within 1 dB of the values we simulated, and the decrease in antenna gain when lowering the antenna from  $0.20\lambda$  to  $0.02\lambda$  is 13.5 dB (open terrain) and 10 dB (tropical forest), respectively. These results align with our findings.

## 7. Conclusion

The relationship between NVIS elevation angles and skip distance is simulated using ionospheric ray tracing software and verified by measurement using a professional RDF. Both measurements and simulations confirm the high elevation angles involved in NVIS, ranging from  $70^\circ$  to  $90^\circ$  for a coverage area with 150-km radius. The measurements show the dominance of NVIS over ground wave propagation starting at a short distance from the transmitter, e.g., 20 km at a frequency of 7 MHz.

For these NVIS elevation angles, the optimum height above ground of horizontal half-wave dipole antennas is sought. To facilitate antenna optimization, NVIS antenna gain and NVIS directivity are defined first as the average gain and average directivity over these NVIS elevation angles ( $70^\circ$  to  $90^\circ$ ). NVIS antenna gain must be optimized for transmission; NVIS directivity must be optimized for best reception.

NEC 4.1 simulations show an optimum NVIS transmit antenna height ranging from  $0.18\lambda$  to  $0.22\lambda$  for most soil types. The NVIS antenna gain at  $0.02\lambda$  is 12 dB lower than the optimum. Above sea water, the optimum height is  $0.13\lambda$ . Simulation shows that the receive antenna height is not critical: NVIS directivity varies only 0.8 dB over a range of  $0.02\lambda$  to  $0.22\lambda$ .

To verify these results, an empirical evaluation method for NVIS antenna performance in the presence of the HF fading

measurement method is proposed and demonstrated. The optimum NVIS transmit antenna height is strongly supported by these measurements. The optimum NVIS receive antenna height found empirically is slightly higher than the simulation suggested, around  $0.16\lambda$  for farmland soil, and is slightly more critical than expected: 2–6-dB deterioration of the SNR occurs when the antenna is lowered to  $0.02\lambda$ .

We may conclude that, in situations where the last few decibels really matter, it is worthwhile to consider the optimum antenna height found here. The difference may be up to 12 dB, which is substantial, and the investment is small. An example could be the establishment of a fixed or ad-hoc base station for emergency communications, which is meant to communicate with small battery-operated stations with suboptimal antennas in the field.

On the other hand, one could conclude that even very low dipole antennas that yield only  $-4.9$  dBi at a height of  $0.02\lambda$  still outperform the  $-17$  dBi of a whip antenna on a car [8]. If propagation is favorable, the 12-dB antenna loss can be offset with an increase in transmit power of the station at the other end of the radio link, provided that station also has the reception capability to match it. However, in any situation where radio communication is essential and peak performance is required, the optima found in this research are recommended.

## 8. Topics for Further Research

Extension of this research, which focused on the horizontal half-wave dipole antenna, to other antenna types is needed. Investigation into the use of arrays of active antennas could further improve the SNR and at the same time reduce cochannel interference by the suppression of signals arriving at lower elevation angles in NVIS reception, as was shown in Section 4.3. Measurements that provide insight in the spatial distribution of ambient noise arriving via skywave, similar to those reported in [18, 19], are helpful input to optimize this aspect of receive antennas. For the same reason, ambient noise measurements in Europe to update ITU-R Recommendation P.372 [16] with more recent man-made noise levels are planned. Research on the use of circular polarization for receive antennas to separately receive the ordinary and extraordinary wave could contribute to fading reduction and diversity reception [33].

## 9. Acknowledgment

The authors would like to thank the Royal Netherlands Army and the personnel of Kamp Holterhoek in Eibergen, The Netherlands, for the use of their property and their practical assistance during the antenna height experiments; J. Mielich of the Leibniz Institute of Atmospheric Physics Kühlungsborn (Juliusruh ionosonde) for providing verified ionosonde data; and also the Radiocommunications Agency Netherlands for the use of their measurement equipment for both the elevation angle and the antenna height experiments.

## 10. References

- [1] M. A. Wallace, "HF radio in Southwest Asia," *IEEE Commun. Mag.*, vol. 30, no. 1, pp. 58–61, Jan. 1992.
- [2] H. Gerritsen, "What happened in 1953? The big flood in the Netherlands in retrospect," *Philos. Trans. Roy. Soc. London A, Math. Phys. Sci.*, vol. 363, no. 1831, pp. 1271–1291, Jun. 2005.
- [3] D. Rollema, "Amateur radio emergency network during 1953 flood," *Proc. IEEE*, vol. 94, no. 4, pp. 759–762, Apr. 2004.
- [4] T. J. Riley, "A comparison of HF digital protocols," in *Proc. Int. Conf. HF Radio Syst. Tech.*, Nottingham, U.K., Jul. 1997, pp. 206–210.
- [5] S. J. Burgess and N. E. Evans, "Short-haul communications using NVIS HF radio," *Electron. Commun. Eng. J.*, vol. 11, no. 2, pp. 95–104, Apr. 1999.
- [6] D. M. Fiedler and E. J. Farmer, *Near Vertical Incidence Skywave Communications, Theory, Techniques and Validation*. Sacramento, CA, USA: Worldradio Books, 1996.
- [7] B. A. Austin and W. C. Liu, "Assessment of vehicle-mounted antennas for NVIS applications," *Proc. Inst. Elect. Eng.—Microw., Antennas Propag.*, vol. 149, no. 3, pp. 147–152, Jun. 2002.
- [8] G. H. Hagn and J. E. Van der Laan, "Measured relative responses toward the Zenith of short-whip antennas on vehicles at high frequency," *IEEE Trans. Veh. Technol.*, vol. VT-19, no. 3, pp. 230–236, Aug. 1970.
- [9] B. A. Austin and K. P. Murray, "Synthesis of vehicular antenna NVIS radiation patterns using the method of characteristic modes," *Proc. Inst. Elect. Eng.—Microw., Antennas Propag.*, vol. 141, no. 4, pp. 151–154, Jun. 1994.
- [10] J. E. Richie and T. Joda, "HF antennas for NVIS applications mounted to helicopters with tandem main rotor blades," *IEEE Trans. Electromagn. Compat.*, vol. 45, no. 2, pp. 444–448, May 2003.
- [11] A. Saakian, "CEM optimization of the HF antennas installations onboard the aircraft," in *Proc. IEEE Int. Symp. Antennas Propag.*, Chicago, Jul. 2012, pp. 1–2.
- [12] R. Vlastic and D. Sumic, "An optimized shipboard HF loop antenna for NVIS link," in *Proc. Int. Symp. ELMAR*, Zadar, Croatia, Sep. 2008, pp. 241–244.
- [13] G. E. Barker, J. Taylor, and G. H. Hagn, "Summary of measurements and modeling of the radiation patterns of simple field antennas in open (level) terrain, mountains and forests," U.S. Army Electronic Command, Aberdeen Proving Ground, MD, USA, Spec. Tech. Rep. 45, December 1971.
- [14] G. E. Barker, "Measurement of the radiation patterns of full-scale HF and VHF," *IEEE Trans. Antennas Propag.*, vol. AP-21, no. 4, pp. 538–544, Jul. 1973.
- [15] G. H. Hagn, "On the relative response and absolute gain toward the Zenith of HF field-expedient antennas—Measured with an ionospheric sounder," *IEEE Trans. Antennas Propag.*, vol. AP-21, no. 4, pp. 571–574, Jul. 1973.
- [16] *Radio Noise*, ITU-R Recommendation P.372-10, International Telecommunication Union (ITU), Oct. 2009.
- [17] E. Van Maanen, "Practical radio noise measurements," in *Proc. Int. Symp. Electromagn. Compat.*, Wroclaw, Poland, Jun. 2006, pp. 427–432.
- [18] L. M. Posa, D. J. Materazzi, and C. Gerson, "Azimuthal variation of measured HF noise," *IEEE Trans. Electromagn. Compat.*, vol. EMC-14, no. 1, pp. 21–31, Feb. 1972.
- [19] C. J. Coleman, "A direction-sensitive model of atmospheric noise and its application to the analysis of HF receiving antennas," *Radio Sci.*, vol. 37, no. 3, pp. 3.1–3.10, May 2002.
- [20] K. G. Budden, *The Propagation of Radio Waves*. Cambridge, U.K.: Cambridge Univ. Press, 1985.
- [21] K. Davies, *Ionospheric Radio*. London, U.K.: Peregrinus, 1990.
- [22] *Internet Space Weather and Radio Propagation Forecasting Course*, Solar Terrestrial Dispatch, Stirling, AB, Canada, 2001.
- [23] S. Chapman, "The atmospheric height distribution of band-absorbed solar radiation," *Proc. Phys. Soc.*, vol. 51, no. 1, pp. 93–109, Jan. 1939.
- [24] S. M. Stankov, J. C. Jodogne, I. Kutiev, K. Stegen, and R. Warnant, "Evaluation of automatic ionogram scaling for use in real-time ionospheric density profile specification: Dourbes DGS-256/ARTIST-4 performance," *Ann. Geophys.*, vol. 55, no. 2, pp. 283–291, 2012.
- [25] E. V. Appleton and G. Builder, "The ionosphere as a doubly-refracting medium," *Proc. Phys. Soc.*, vol. 45, no. 2, pp. 208–220, Mar. 1933.
- [26] M. C. Walden, "The extraordinary wave mode: Neglected in current practical literature for HF NVIS communications," in *Proc. Int. Conf. Ionospheric Radio Syst. Tech.*, Edinburgh, U.K., Apr. 2009, pp. 1–5.
- [27] W. Webber, "The production of free electrons in the ionospheric D layer by solar and galactic cosmic rays and the resultant absorption of radio waves," *J. Geophys. Res.*, vol. 67, no. 13, pp. 5091–5106, Dec. 1962.
- [28] S. L. Ossakow, "Spread-F theories—A review," *J. Atmos. Terrestrial Phys.*, vol. 43, no. 5/6, pp. 437–452, May/Jun. 1981.
- [29] D. F. Martyn, R. O. Cherry, and A. L. Green, "Long-distance observations of radio waves of medium frequencies," *Proc. Phys. Soc.*, vol. 47, no. 2, pp. 323–340, Mar. 1935.
- [30] N. Smith, "The relation of radio skywave transmission to ionosphere measurements," *Proc. IRE*, vol. 27, no. 5, pp. 332–347, May 1939.
- [31] *Proplab-Pro Version 3*, Solar Terrestrial Dispatch, Stirling, AB, Canada, [Online]. Available: <http://www.spacew.com/proplab/index.html>.
- [32] B. A. Witvliet, E. van Maanen, A. J. Westenberg, and G. Visser, "Elevation angle measurements for NVIS propagation," *RadCom*, vol. 81, no. 6, pp. 76–79, Jun. 2005.
- [33] B. A. Witvliet et al., "The importance of circular polarization for diversity reception and MIMO in NVIS propagation," in *Proc. Eur. Conf. Antennas Propag.*, Hague, The Netherlands, Apr. 2014, pp. 2797–2801.
- [34] J. D. Kraus, *Antennas*. 2nd ed. New York, NY, USA: McGraw-Hill, 1988.
- [35] G. J. Burke, E. K. Miller, and A. I. Poggio, "The Numerical Electromagnetics Code (NEC)—A brief history," in *Proc. IEEE Int. Symp. Antennas Propag.*, Jun. 2004, vol. 3, pp. 2871–2874.
- [36] G. J. Burke et al., "Computer modeling of antennas near the ground," *Electromagnetics*, vol. 1, no. 1, pp. 29–49, Jan. 1981.
- [37] B. D. Van Veen and K. M. Buckley, "Beamforming: A versatile approach to spatial filtering," *IEEE ASSP Mag.*, vol. 5, no. 2, pp. 4–24, Apr. 1988.
- [38] J. L. Sanz-González, S. Zazo-Bella, I. A. Perez-Alvarez, and J. Lopez-Perez, "Parameter estimation algorithms for ionospheric channels," in *Proc. Int. Conf. Ionospheric Radio Syst. Tech.*, Edinburgh, U.K., Apr. 2009, pp. 1–5.
- [39] W. N. Furman and E. Koski, "Standardization of an intermediate duration HF channel variation model," in *Proc. Int. Conf. Ionospheric Radio Syst. Tech.*, Edinburgh, U.K., Apr. 2009, pp. 1–5.
- [40] A. G. Ads, "*Soundings of the ionospheric HF radio link between Antarctica and Spain*," Ph.D. dissertation, Univ. Ramon Llull, Barcelona, Spain, 2013.
- [41] *R&S FSMR Measuring Receiver, Data Sheet Version 7.00*, Rohde & Schwarz, München, Germany, Jan. 2009.
- [42] B. A. Austin, "Optimum Antenna Height for Single-Hop Oblique Incidence (NVIS) Propagation," [Online]. Available: [http://www.ips.gov.au/IPSHosted/INAG/web-70/2009/optimum\\_antenna\\_height.pdf](http://www.ips.gov.au/IPSHosted/INAG/web-70/2009/optimum_antenna_height.pdf).



**Ben A. Witvliet**, (M'09 - SM'11) was born in Biak, Netherlands New Guinea in 1961. He received his BSc in Electronics and Telecommunications in 1988 in Enschede, The Netherlands. He has working experience in electrical and electronic maintenance in Israel, in international telecommunication network management in The Netherlands, as Chief Engineer of the high power shortwave radio station of Radio Netherlands World Service in Madagascar and as manager of a team of technical specialists for TV, FM and AM broadcast transmitter operator NOZEMA in The Netherlands. Since 1997 he works for Radiocommunications Agency Netherlands, currently as Technical Advisor. Research conducted for the Radiocommunications Agency includes long term long distance UHF propagation measurements, the design and realization of a helicopter-based system to measure antenna diagram and effective isotropically radiated power of FM broadcast stations, electromagnetic HF background noise measurement and UHF antenna gain measurements. Since 2011 he is combines his work with part-time PhD research in the Telecommunication Engineering group of the University of Twente, The Netherlands. His research topic is Near Vertical Incidence Skywave antenna and propagation interaction and its application to emergency communications. He is a Senior Member of the IEEE Antennas and Propagation Society and member of European Association on Antennas and Propagation (EurAAP).



**Erik van Maanen**, born in 1963 in Leiden, The Netherlands, studied Electronics in Leiden. He worked for Delft University of Technology for 5 years and for the Radiocommunications Agency Netherlands since 1993, currently as Technical Advisor. His areas of expertise are Short Range Devices, antenna technology, digital signal processing, measurements, instrument control and simulation and scenario tools. He was contributor and chapter coordinator of the Spectrum Monitoring Handbooks 1995-2005 of the International Telecommunication Union

(ITU), and authored ITU-R Recommendations on Helicopter Antenna Measurements and Radio Noise Measurements. He participates in a large number of international working parties on radio equipment standardization and frequency management. He took part in most of the research projects mentioned above in the biography of Ben Witvliet.



**George J. Petersen**, born 1961 in Leeuwarden, The Netherlands, studied Telecommunications at the Royal Military Academy (1989). He worked at several positions in the Ministry of Defense. Since 1998 he works for the Radiocommunications Agency Netherlands, currently as Specialist Public Safety. He holds a MSc in Business Management from Radboud University (2004).



**Albert J. Westenberg**, born in The Hague 1949, studied Electronics in The Hague and served the Dutch Navy for 21 months. He worked as development engineer at a laboratory of the Ministry of Defense for almost 8 years. In 1978 he started working for the Radiocommunications Agency Netherlands. Until his retirement in 2005 he was involved in maritime regulations, including equipment type approval, frequency planning and international coordination.



**Mark J. Bentum**, (S'92, M'95, SM'09) was born in Smilde, The Netherlands, in 1967. He received the MSc degree in Electrical Engineering (with honors) from the University of Twente, Enschede, The Netherlands, in August 1991. In December 1995 he received the PhD degree, also from the University of Twente. From December 1995 to June 1996 he was a research assistant at the University of Twente in the field of signal processing for mobile telecommunications and medical data processing. In June 1996 he joined the Netherlands Foundation for Research in Astronomy (ASTRON). He was in various positions at ASTRON. In 2005 he was involved in the eSMA project in Hawaii to correlate the Dutch JCMT mm-telescope with the Submillimeter Array (SMA) of Harvard University. From 2005 to 2008 he was responsible for the construction of the first software radio telescope in the world, LOFAR (Low Frequency Array). In 2008 he became an Associate Professor in the Telecommunication Engineering Group at the University of Twente. He is now involved with research and education in mobile radio communications. His current research interests are short-range radio communications, novel receiver technologies (for instance in the field of radio

astronomy), channel modeling, interference mitigation, sensor networks and aerospace. Dr. Bentum is a Senior Member of the IEEE, Chairman of the Dutch URSI committee, initiator and chair of the IEEE Benelux AES/GRSS chapter, board member of the Dutch Electronics and Radio Society NERG, board member of the Dutch Royal Institute of Engineers KIVI NIRIA, member of the Dutch Pattern Recognition Society, and has acted as a reviewer for various conferences and journals. Since December 2013 he is also the program director of Electrical Engineering at the University of Twente.

astronomy), channel modeling, interference mitigation, sensor networks and aerospace. Dr. Bentum is a Senior Member of the IEEE, Chairman of the Dutch URSI committee, initiator and chair of the IEEE Benelux AES/GRSS chapter, board member of the Dutch Electronics and Radio Society NERG, board member of the Dutch Royal Institute of Engineers KIVI NIRIA, member of the Dutch Pattern Recognition Society, and has acted as a reviewer for various conferences and journals. Since December 2013 he is also the program director of Electrical Engineering at the University of Twente.



**Cornelis H. Slump**, received the M.Sc. degree in Electrical Engineering from Delft University of Technology, the Netherlands in 1979. In 1984 he obtained his Ph.D. in physics from the University of Groningen, the Netherlands. From 1983 to 1989 he was employed at Philips Medical Systems in Best, The Netherlands as head of a predevelopment group on X-ray image quality and cardiovascular image processing. In 1989 he joined the Department of Electrical Engineering from the University of Twente, Enschede, The Netherlands. In June 1999 he

was appointed as a full professor in signal processing. His main research interest is in detection and estimation, interference reduction, pattern analysis and image analysis as a part of medical imaging. He is a member of IEEE and SPIE.



**Roel Schiphorst**, received his M.Sc. degree with honours in Electrical Engineering from the University of Twente in 2000 for his research on Software-Defined Radio. In 2004 he received the PhD degree for his research on Software-Defined Radio for WLAN standards. From 2004 to 2014 he has been a senior researcher of the chair Signals and Systems. He is author or co-author of over 70 papers, published in technical journals or presented at international symposia. His research interests include: coexistence studies in wireless applications and digital signal

processing in wireless communication (physical layer). Roel is member of IEEE, COST-TERRA, Network of Excellence ICT ACROPOLIS and CR-platform NL. Since 2013 Roel is working for BlueMark Innovations; a spin-off of the University of Twente which he has founded in 2009. BlueMark Innovations is a technology firm that specializes in detecting and locating smartphones. 